Chinese Chemical Letters 33 (2022) 3709–3712

Contents lists available at ScienceDirect

Chinese Chemical Letters

journal homepage: www.elsevier.com/locate/cclet

Facilely anchoring Cu_2O nanoparticles on mesoporous TiO_2 nanorods for enhanced photocatalytic CO_2 reduction through efficient charge transfer

Ge Yang[a], Pei Qiu[a], Jinyan Xiong[b], Xueteng Zhu[a], Gang Cheng[a,*]

[a] School of Chemistry and Environmental Engineering, Wuhan Institute of Technology, Donghu New & High Technology Development Zone, Wuhan 430205, China

[b] College of Chemistry and Chemical Engineering, Wuhan Textile University, Wuhan 430200, China

ARTICLE INFO

Article history:
Received 14 August 2021
Revised 15 September 2021
Accepted 18 October 2021
Available online 23 October 2021

Keywords:
TiO_2/Cu_2O composite
Photocatalytic CO_2 reduction
Photocatalysis
Charge separation
p-n Junction

ABSTRACT

Semiconductor-employed photocatalytic CO_2 reduction has been regarded as a promising approach for environmental-friendly conversion of CO_2 into solar fuels. Herein, TiO_2/Cu_2O composite nanorods have been successfully fabricated by a facile chemical reduction method and applied for photocatalytic CO_2 reduction. The composition and structure characterization indicates that the Cu_2O nanoparticles are coupled with TiO_2 nanorods with an intimate contact. Under light illumination, all the TiO_2/Cu_2O composite nanorods enhance the photocatalytic CO_2 reduction. In particular, the TiO_2/Cu_2O-15% sample exhibits the highest CH_4 yield (1.35 μmol g^{-1} h^{-1}) within 4 h irradiation, and it is 3.07 and 15 times higher than that of pristine TiO_2 nanorods and Cu_2O nanoparticles, respectively. The enhanced photoreduction capability of the TiO_2/Cu_2O-15% is attributed to the intimate construction of Cu_2O nanoparticles on TiO_2 nanorods with formed p-n junction to accelerate the separation of photogenerated electron-hole pairs. This work provides a reference for rational design of a p-n heterojunction photocatalyst for CO_2 photoreduction.

Photocatalytic CO_2 reduction into solar fuels has attracted increasing attention because it is a compelling approach to tackle the issues of greenhouse gas global warming and energy shortage we are currently facing [1–8]. It is of significance to develop stable and highly-active photocatalysts which process the characteristics of good CO_2 adsorption and solar light harvesting, rapid charge transfer, and strong surface reaction capability [9–16]. Among various semiconductor photocatalysts, Cu_2O is a typical p-type one with a narrow band gap (~2.2 eV). It can be excited by the visible light and has more negative conduction band position, and therefore it has great potential in solar-driven CO_2 photoreduction [17–20]. At the same time, n-type semiconductor TiO_2 has also been widely studied due to its non-toxic, low-cost, and suitable band structure, although it can only absorb the UV light [21–24]. However, both of the TiO_2 and Cu_2O suffer from the limitation of rapid recombination of photogenerated electron-hole pairs, resulting in a low photocatalytic performance [25–28].

As a matter of fact, when combining the p-type Cu_2O with the n-type TiO_2 to construct a hybrid with a good contact, a p-n junction would be formed between p-Cu_2O and n-TiO_2 upon light irradiation. In this case, an inner electric field would be built in such formed hybrid, which facilitates the separation of the photoinduced electrons and holes, leading to an efficient photocatalysis [29,30]. In recent years, Cu_2O/TiO_2 p-n junction was widely used as an efficient photocatalyst for organic pollutants degradation [31–36] and splitting water to hydrogen [37–39]. However, there are few reports relevant to CO_2 photoreduction upon the TiO_2/Cu_2O composite. Bi *et al.* [40] and Xu *et al.* [41] recently reported efficient CO_2 photoreduction was achieved through employing porous Cu_2O/TiO_2 p-n junction as the photocatalyst. However, it is still a great challenge to develop a facile approach to prepare TiO_2/Cu_2O heterojunction with a good contact for a high-active photocatalyst.

On the basis of the above background, in this work, the composite of mesoporous TiO_2 nanorods coupled with Cu_2O nanoparticles has been successfully prepared by a facile chemical reduction method. The composition and structure of the as-synthesized TiO_2/Cu_2O composite were characterized. The enhanced photoreduction capability of the TiO_2/Cu_2O composite was also studied.

The TiO_2/Cu_2O composite was fabricated according to the schemed process displayed in Scheme 1, in which TiO_2 nanorods are firstly prepared and subsequently anchoring Cu_2O nanoparti-

* Corresponding author.
E-mail address: gchenglab@163.com (G. Cheng).

https://doi.org/10.1016/j.cclet.2021.10.047
1001-8417/

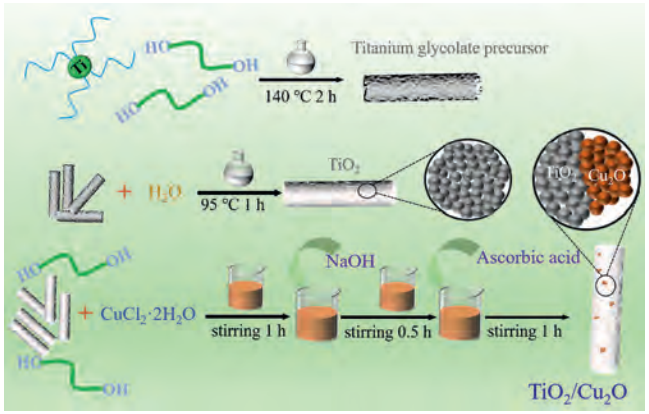

Scheme 1. Illustration for fabrication of TiO_2/Cu_2O composite, where titanium glycolate precursor and TiO_2 nanorods preparation was involved.

cles on its surface. XRD pattern obtained for titanium glycolate precursor is shown in Fig. S1a (Supporting information), which displays amorphous characteristics [42]. As shown in Fig. S1b (Supporting information), the as-prepared titanium glycolate precursor is composed of rod-like nanostructures with a length of 2–6 μm and diameter of 0.7–2 μm. As can be seen in Fig. S1c (Supporting information), the inside of the titanium glycolate precursor is solid. Fig. S2a (Supporting information) shows the XRD pattern of the TiO_2 prepared from titanium glycolate precursor, and it can be seen that the diffraction peaks belong to the standard pattern (JCPDS No. 4–477) of anatase TiO_2. As shown in Figs. S2b and c (Supporting information), after refluxing 95 °C for 1 h, the as-prepared TiO_2 still keeps a rod-like structure, and the nanorod is comprised of nanoparticles, and accordingly forms a mesoporous structure. Fig. S3a (Supporting information) shows the XRD pattern of the as-synthesized Cu_2O, all the peaks match well with cuprite Cu_2O (JCPDS No. 5–667). As can be seen in Figs. S3b and c (Supporting information), the as-synthesized Cu_2O are nanoparticles with a size of 20–50 nm.

Fig. 1a shows the XRD patterns of the TiO_2/Cu_2O composites. It can be seen that all the diffraction peaks can be indexed to anatase TiO_2 (JCPDS No. 4–477) and Cuprite Cu_2O (JCPDS No. 5–667). With increasing Cu_2O anchoring, the TiO_2/Cu_2O composite obviously exhibits the characteristic peaks of Cu_2O in XRD pattern. Fig. 1b shows the UV-DRS spectrum of the as-prepared products. TiO_2 displays the characteristic absorption edge at about 389 nm. With increasing Cu_2O anchoring, all the composites show the enhanced absorption intensity in the visible light region from 400 nm to 800 nm.

The composition and states of elements for TiO_2, Cu_2O, and the TiO_2/Cu_2O composite are analyzed by the X-ray photoelectron spectroscopy (XPS). As depicted in Fig. 1c, Ti and O elements exist in the TiO_2 sample, and Cu and O elements exist in the Cu_2O sample. For the TiO_2/Cu_2O-15% sample, Ti, Cu and O elements can be observed. Fig. 1d shows the high-resolution XPS spectrum of Cu 2p. The binding energy of 932.3 and 952.2 eV is attributed to Cu $2p_{3/2}$ and Cu $2p_{1/3}$ of Cu_2O, respectively [43,44]. The peaks at binding energy of 934.2, 942.0, and 953.9 eV show the appearance of CuO in the sample [45–47]. Fig. 1e shows the high-resolution XPS spectrum of Ti 2p. The two typical binding energies at ~458.2 and ~464.0 eV can be attributed to the Ti $2p_{3/2}$ and Ti $2p_{1/2}$, respectively, indicating the existence of Ti^{4+} in the TiO_2 and the TiO_2/Cu_2O-15% samples [25,48]. Fig. 1f displays the high-resolution XPS spectrum of O 1s. For the TiO_2 and the TiO_2/Cu_2O-15% samples, the peaks located at 530.0 and 531.2 eV correspond to the lattice oxygen and the surface hydroxyl groups [49,50]. For the Cu_2O sample, the main peak is located at 530.7 eV, which is a signal of surface absorbed oxygen molecule [46]. It can be observed that the Ti 2p and Cu 2p bind energy of the TiO_2/Cu_2O-15% sample shift to the higher one, compared with pristine TiO_2 and Cu_2O. This result indicates an interaction exists between the Cu_2O and TiO_2. In other words, when the p-type Cu_2O and n-type TiO_2 have an intimate contact, a heterojunction could be formed, and an electron transfer could occur from the p-type Cu_2O to n-type TiO_2 until the system keeps equilibration [51].

The morphology of the TiO_2/Cu_2O-15% composite is further observed by SEM images. As displayed in Figs. 2a and b, the composite still keeps the same rod-like structure as the TiO_2 supporter, while the Cu_2O nanoparticles are deposited on the surface of the rods (Fig. 2c). EDX mapping was performed to get more information to confirm the composition of the TiO_2/Cu_2O composite. As shown in Figs. 2d-h, the red, green, and blue colors represent the existence and distributions of O, Ti and Cu, respectively. It can be seen that Cu_2O is uniformly coated on the TiO_2 nanorods. This result further confirms the TiO_2/Cu_2O composite has been successfully prepared by such a facile chemical reduction method.

The photocatalytic CO_2 reduction performance of the as-prepared samples are evaluated under 300 W Xe lamp irradiation, and the gas products were detected by gas chromatography. As dis-

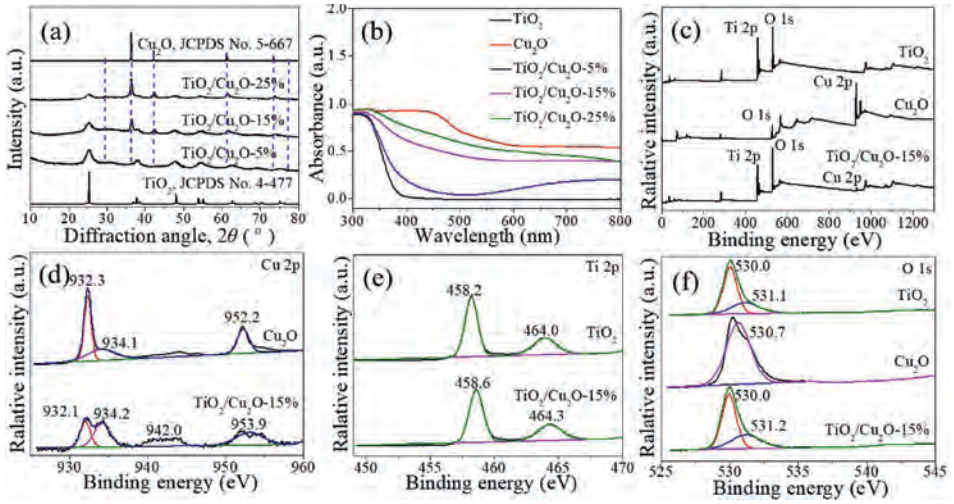

Fig. 1. (a) XRD patterns of the TiO_2/Cu_2O composites. (b) UV-DRS spectra of the TiO_2, Cu_2O and TiO_2/Cu_2O composites. (c) XPS survey spectra of TiO_2, Cu_2O and TiO_2/Cu_2O-15% samples; high-resolution XPS spectra of (d) Cu 2p, (e) Ti 2p and (f) O 1s for different samples.

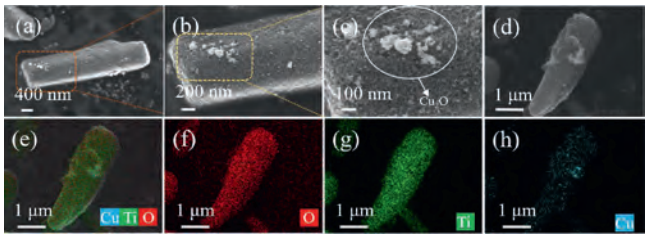

Fig. 2. (a-c) SEM images of the TiO_2/Cu_2O-15% sample; (d-h) SEM image of the TiO_2/Cu_2O-15% sample and its EDX mapping images of O, Ti, and Cu elements.

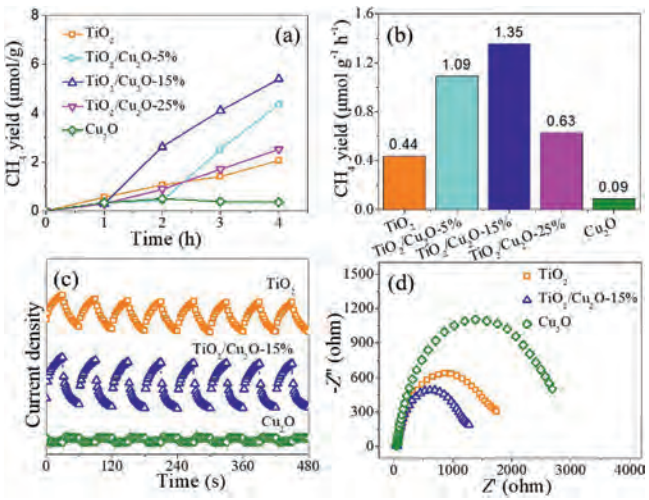

Fig. 3. Photocatalytic CO_2 reduction activity (a) and production rates (b) of TiO_2, TiO_2/Cu_2O-5%, TiO_2/Cu_2O-15%, TiO_2/Cu_2O-25%, and Cu_2O under light irradiation; (c) transient photocurrent responses and (d) electrochemical impedance spectra of TiO_2, TiO_2/Cu_2O-15%, and Cu_2O samples.

played in Fig. 3a, the pristine Cu_2O nanoparticles almost have no activity towards photocatalytic CO_2 reduction under light irradiation within 4 h. Compared with pristine TiO_2, the TiO_2/Cu_2O composites can enhance the photocatalytic performance for CO_2 reduction. Among the different composites, the TiO_2/Cu_2O-15% shows the highest activity. As shown in Fig. 3b and Fig. S4 (Supporting information), within 4 h light illumination, the TiO_2/Cu_2O-15% sample exhibits the CH_4 yield with a rate of 1.35 μmol g^{-1} h^{-1}, which is 3.1 and 15.0 folds higher than that of pure TiO_2 and pure Cu_2O samples, respectively. As shown in Fig. S5 (Supporting information), the XRD pattern of the TiO_2/Cu_2O-15% after reaction correspond well to the standard Cu_2O (JCPDS No. 5-667) and TiO_2 (JCPDS No. 5-667), indicating that the TiO_2/Cu_2O-15% sample keeps the same composition before and after reaction. Recently Xu and co-workers [52] found the formation of Cu(I)/Cu(0) from the initial atomically dispersed Cu(II) was proposed to be more effective for CH_4 formation. In present work, as shown in Fig. S6a (Supporting information), with increasing of recycling test times, the yield of CH_4 decreases, and it is 0.59 μmol g^{-1} h^{-1} after four cycles. The XRD pattern of the as-cycled TiO_2/Cu_2O-15% sample is shown in Fig. S6b (Supporting information), it is found that the diffraction peaks of the Cu_2O disappear. It might result in the decrease of the catalytic performance. Further study is underway.

Photo/electrochemical measurements are performed to study the interfacial charge transfer of the above photocatalysts, which has a significant impact on the photocatalytic performance [52–56]. As shown in Fig. 3c, the TiO_2/Cu_2O-15% sample exhibits superior photocurrent intensity than the pristine TiO_2 and Cu_2O, and it indicates the composite has enhanced capability of electron-hole pairs separation. Fig. 3d reveals the electrochemical impedance

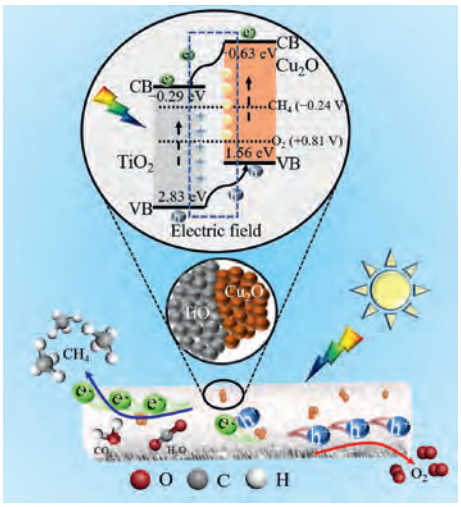

Scheme 2. Schematic illustration of photocatalytic CO_2 reduction upon the TiO_2/Cu_2O composite.

spectra (EIS) of the TiO_2, Cu_2O, and TiO_2/Cu_2O-15% samples. It can be obviously observed that the TiO_2/Cu_2O-15% sample has the smallest semicircle, suggesting the smallest resistance existence and rapid charge transfer at the interface of the TiO_2/Cu_2O-15% sample.

Taking into the band structure of the photocatalyst is related to the thermodynamics of the CO_2 photoreduction. UV–vis diffuse reflectance spectroscopy and valence-band XPS spectrum were employed to determine the band gap energy and the valence band position of the samples. As shown in Fig. S7 (Supporting information), the band gap of TiO_2 and Cu_2O calculated from the Kubelka-Munk function is 3.12 and 2.19 eV, respectively. As displayed in Fig. S8 (Supporting information), according to the valence-band XPS spectrum, the valence band position for TiO_2 and Cu_2O is 2.83 and 1.56 eV, respectively.

Based on the above results, the conduction band of TiO_2 and Cu_2O is calculated to be −0.29 and −0.63 eV *vs.* NHE (pH 0), respectively. As mentioned in the XPS result and reported previously [34,36,39], the p-n heterojunction would be formed when the TiO_2 and Cu_2O have an intimate contact. In this case, as shown in Scheme 2, the diffusion of electrons from Cu_2O to TiO_2 could occur, while the holes diffuse from TiO_2 to Cu_2O. Accordingly, an internal electric field from n-type TiO_2 to p-type Cu_2O would be established. Under light illumination, photogenerated electron-hole pairs would be produced due to the excitation of TiO_2 and Cu_2O, and the formed internal electric field would facilitate the migration of electrons to the TiO_2 and the transfer of holes to Cu_2O. In this regard, efficient charge separation would be achieved. Finally, more photoinduced electrons would participate in the photocatalysis process, and the photocatalytic CO_2 reduction to CH_4 is improved.

In summary, a facile chemical reduction method has been used to fabricate the TiO_2/Cu_2O composite, in which the Cu_2O nanoparticles couple with the TiO_2 nanorods. Under light illumination, the TiO_2/Cu_2O composites show superior performance than TiO_2 and Cu_2O towards photocatalytic CO_2 reduction to CH_4. The TiO_2/Cu_2O-15% composite exhibits the highest CH_4 yield rate of 1.35 μmol g^{-1} h^{-1} within 4 h. Based on the XPS, band structure, and photo/electrochemical measurements, the TiO_2/Cu_2O composite with an intimate contact would allow the establishment of internal electric field, which greatly improves the separation and migration of photoinduced charge carriers, and therefore promotes photoreduction of CO_2 into CH_4. It is expected that this work could

offer an efficient approach to design p-n junction for CO_2 photoreduction.

Declaration of competing interest

The authors declare that they have no known competing financial interests or personal relationships that could have appeared to influence the work reported in this paper.

Acknowledgment

This work was supported by the National Natural Science Foundation of China (No. 21501137).

Supplementary materials

Supplementary material associated with this article can be found, in the online version, at doi:10.1016/j.cclet.2021.10.047.

References

[1] T. Kong, Y. Jiang, Y. Xiong, Chem. Soc. Rev. 49 (2020) 6579–6591.
[2] L. Liu, S. Wang, H. Huang, et al., Nano Energy 75 (2020) 104959.
[3] X. Wu, C. Wang, Y. Wei, et al., J. Catal. 377 (2019) 309–321.
[4] W. He, X. Wu, Y. Li, et al., Chin. Chem. Lett. 31 (2020) 2774–2778.
[5] H. Yang, C. He, L. Fu, et al., Chin. Chem. Lett. 32 (2021) 3202–3206.
[6] L. Fu, R. Wang, C. Zhao, et al., Chem. Eng. J. 414 (2021) 128857.
[7] F. Zhang, Y.H. Li, M.Y. Qi, et al., Chem Catal. 1 (2021) 272–297.
[8] G. Yang, X. Zhu, G. Cheng, et al., J. Mater. Chem. A 9 (2021) 22781–22809.
[9] J. Ran, M. Jaroniec, S.Z. Qiao, Adv. Mater. 30 (2018) 1704649.
[10] L. Yu, G. Li, X. Zhang, et al., ACS Catal. 6 (2016) 6444–6454.
[11] R. Wang, C. He, W. Chen, et al., Chin. Chem. Lett. 32 (2021) 3821–3824.
[12] J. Xiong, M. Zhang, M. Lu, et al., Chin. Chem. Lett. 33 (2022) 1313–1316.
[13] Y. Xi, X. Zhang, Y. Shen, et al., Appl. Catal. B 297 (2021) 120411.
[14] S. Zhong, Y. Xi, Q. Chen, et al., Nanoscale 12 (2020) 5764–5791.
[15] Y. Xi, W. Chen, W. Dong, et al., ACS Appl. Mater. Interfaces 13 (2021) 39491–39500.
[16] S. Liu, Z.R. Tang, Y. Sun, et al., Chem. Soc. Rev. 44 (2015) 5053–5075.
[17] Y.A. Wu, I. McNulty, C. Liu, et al., Nat. Energy 4 (2019) 957–968.
[18] S. Ali, J. Lee, H. Kim, et al., Appl. Catal. B 279 (2020) 119344.
[19] Y. Pu, Y. Luo, X. Wei, et al., Appl. Catal. B 254 (2019) 580–586.
[20] J.Y. Li, L. Yuan, S.H. Li, et al., J. Mater. Chem. A 7 (2019) 8676–8689.
[21] W.J. Yin, B. Wen, C. Zhou, et al., Surf. Sci. Rep. 73 (2018) 58–82.
[22] Q.D. Truong, H.T. Hoa, T.S. Le, J. Colloid Interface Sci. 504 (2017) 223–229.
[23] L. Liu, Y. Jiang, H. Zhao, et al., ACS Catal. 6 (2016) 1097–1108.
[24] C. Wang, Y. Zhao, H. Xu, et al., Appl. Catal. B 263 (2020) 118314.
[25] Y. Sun, G. Li, Y. Gong, et al., J. Hazard. Mater. 403 (2021) 124019.
[26] S. Zhu, X. Chen, Z. Li, et al., Appl. Catal. B 264 (2020) 118515.
[27] L. Yu, X. Ba, M. Qiu, et al., Nano Energy 60 (2019) 576–582.
[28] C. Wang, X. Liu, W. He, et al., J. Catal. 389 (2020) 440–449.
[29] L. Bai, H. Huang, S. Zhang, et al., Adv. Sci. 7 (2020) 2001939.
[30] F. Nekouei, S. Nekouei, M. Pouzesh, et al., Chem. Eng. J. 385 (2020) 123710.
[31] G.R. Surikanti, A.K. Bandarapu, M.V. Sunkara, ChemistrySelect 4 (2019) 2249–2257.
[32] X. Liu, L. Cao, W. Sun, et al., Res. Chem. Intermed. 42 (2016) 6289–6300.
[33] X. Fei, F. Li, L. Cao, et al., Mater. Sci. Semicond. Process. 33 (2015) 9–15.
[34] L. Li, J. Lei, T. Ji, Mater. Res. Bull. 46 (2011) 2084–2089.
[35] R.C. Ding, Y.Z. Fan, G.S. Wang, ChemistrySelect 3 (2018) 1682–1687.
[36] L. Liu, W. Yang, W. Sun, et al., ACS Appl. Mater. Interfaces 7 (2015) 1465–1476.
[37] P.A. Bharad, A.V. Nikam, F. Thomas, et al., ChemistrySelect 3 (2018) 12022–12030.
[38] K. Yang, G. Cheng, R. Chen, et al., Energy Technol (2021), doi:10.1002/ente.202100259.
[39] Y. Li, B. Wang, S. Liu, et al., Appl. Surf. Sci. 324 (2015) 736–744.
[40] F. Bi, M.F. Ehsan, W. Liu, et al., Chin. J. Chem. 33 (2015) 112–118.
[41] H. Xu, S. Ouyang, L. Liu, et al., Nanotechnology 25 (2014) 165402.
[42] Y. Wei, G. Cheng, J. Xiong, et al., J. Energy Chem. 32 (2019) 45–56.
[43] F. Li, L. Zhang, J. Tong, et al., Nano Energy 27 (2016) 320–329.
[44] Z. Zeng, Y. Yan, J. Chen, et al., Adv. Funct. Mater. 29 (2019) 1806500.
[45] X. An, K. Li, J. Tang, ChemSusChem 7 (2014) 1086–1093.
[46] Z. Sun, W. Fang, L. Zhao, et al., Environ. Int. 130 (2019) 104898.
[47] M. Bersani, K. Gupta, A.K. Mishra, et al., ACS Catal. 6 (2016) 5823–5833.
[48] A. Razzaq, A. Sinhamahapatra, T.H. Kang, et al., Appl. Catal. B 215 (2017) 28–35.
[49] M. Trejo-Valdez, S.R. Hernández-Guzmán, M.E. Manriquez-Ramírez, et al., J. Hazard. Mater. 370 (2019) 196–202.
[50] J.Z.Y. Tan, F. Xia, M.M. Maroto-Valer, ChemSusChem 12 (2019) 5246–5252.
[51] Z. Zhang, C. Shao, X. Li, et al., ACS Appl. Mater. Interfaces 2 (2010) 2915–2923.
[52] L. Yuan, S.F. Hung, Z.R. Tang, et al., ACS Catal. 9 (2019) 4824–4833.
[53] H. Gao, J. Wang, M. Jia, et al., Chem. Eng. J. 374 (2019) 684–693.
[54] Y. Ma, Q. Tang, W.Y. Sun, et al., Appl. Catal. B 270 (2020) 118856.
[55] J. Xiong, M. Zhang, G. Cheng, J. Colloid Interface Sci. 579 (2020) 872–877.
[56] L. Yuan, K.Q. Lu, F. Zhang, et al., Appl. Catal. B 237 (2018) 424–431.